Intracellular-Molecule Changes in Plasma-irradiated Budding Yeast Cells Using Multiplex Coherent Anti-Stokes Raman Scattering Microscopy

Ryo Furuta,[a] Naoyuki Kurake,[a] Kenji Ishikawa,[a] Keigo Takeda,[a] Hiroshi Hashizume,[a] Hiroki Kondo,[a] Takayuki Ohta,[b] Masafumi Ito,[b] Makoto Sekine [a] and Masaru Hori [a]

[a] Graduate School of Engineering, Nagoya University, Furo-cho Chikusa-ku, Nagoya 464-8603, Japan

[b] Graduate School of Science & Technology, Meijo University, 1-501 Shiogamaguchi Tenpaku-ku, Nagoya 468-8502, Japan

E-mail: furuta.ryou@j.mbox.nagoya-u.ac.jp

Interactions between non-equilibrium atmospheric-pressure plasma (NEAPP) and living cells were examined using multiplex coherent anti-Stokes Raman scattering (CARS) microscopy. Our multiplex CARS analyses revealed that NEAPP irradiation generates short-lived radicals that induce decrease in mitochondrial activity of budding yeast cells. By manipulating electron dynamics controlled by oscillating electromagnetic fields, we can produce non-equilibrium plasma even under normal atmospheric pressure and temperature (known as cold atmospheric plasma or non-equilibrium atmospheric-pressure plasma [NEAPP]). This type of plasma does not produce any thermal damage when interacting with living organisms or cells.

A number of medical applications of NEAPP have been reported in recent years. For example, NEAPP is used to sterilize medical instruments,[1] introduce hydrophilic or hydrophobic modifications on the surface of medical instruments,[2] promote wound healing,[3] and selectively kill cancer cells.[4] Iseki *et al*. reported that direct NEAPP irradiation of ovarian cancer cells and normal fibroblast cells in suspension results in selective killing of the cancer cells due to activation of programmed cell death processes (i.e., apoptosis).[5] The reactive oxygen and nitrogen species (RONS) generated by NEAPP irradiation can significantly affect a variety of biological processes,[6,7] and plasma-generated ultraviolet (UV) emissions affect the biological functions of cancer cells.[8] Fully elucidating the effect of NEAPP irradiation on complex biological/physiological processes and responses, however, requires a thorough understanding of how NEAPP affects biochemical reactions.

Fluorescence microscopy enables the visualization of intracellular reactions and morphologic changes in cells subjected to specific staining.[9,10] However, fluorescent labelling has several disadvantages. For example, the process is time consuming, and the dynamic behavior of living cells[11] or the effects of photo-bleaching or other perturbations[12] cannot be observed. Raman scattering microscopy, by contrast, carries the advantage of enabling label-free detection of molecular vibrations within a cell.[13] Detecting spontaneous Raman scattering signals originating from living cells is difficult, however, because these signals are generally weaker than auto-fluorescence signals.[13,14] Irradiation utilizing coherent anti-Stokes Raman scattering (CARS) is an alternative that provides significantly enhanced emission of scattering signals, thus enabling the discrimination of molecular species.[13,14] CARS mapping can therefore be used to examine the morphology of living cells. Another advantage of CARS is that

signals can be isolated and thus analyzed without interference from auto-fluorescence.[14,15]

The CARS technique also provides enhanced sensitivity. CARS signals exhibit the characteristics of a third-order nonlinear optical process.[12,15] Multiplex CARS enables the simultaneous measurement of a wide spectral range through the use of a broadband super-continuum light for the Stokes laser in conjunction with dispersive optics with an array detector.[15] The use of CARS for spatial scanning of samples on a rapidly moving stage enables spectral mapping, which is suitable for microscopic imaging of the structures of living cells, such as the cell membrane, organelles, and nucleus.[13-15] These advantages make multiplex CARS microscopy an ideal technique for the high-sensitivity, label-free measurement of molecular vibrations in living cells and organisms.

Many reports of the use of CARS to observe living cells have been reported. Using multiplex CARS microscopy, Hamaguchi *et al*. identified a unique Raman band at 1602 cm^{-1} that is associated with the mitochondria in living fission yeast and budding yeast cells.[16,17] This band was designated the “Raman spectroscopic signature of life,” and its intensity is generally interpreted as reflecting the metabolic activity of the mitochondria in living yeast cells. Reports describing the effects of the addition of nutrients to cells grown in YE medium18 and the inhibition of respiration in the presence of KCN support the biological importance of this band.[17]

In this study, we examined the effects of NEAPP irradiation on biochemical reactions occurring in budding yeast cells as a model eukaryote. Yeasts are used as models of eukaryotic cells due to their size (approximately 5 μm), and their intracellular organelles are commonly used to study the biology and biochemistry of higher plants

and animal cells.[19] Budding yeasts can also be used to model the effects of interactions of cancer cells with plasmas. Here, we report the two-dimensional mapping of NEAPP plasma–irradiated budding yeast cells using multiplex CARS microscopy. This approach permitted the label-free analysis of chemical vibrations originating from the phospholipids, organelles, and nucleus. The effects on budding yeast cells of short- and long-lived chemical species generated by NEAPP irradiation are described.

Figure 1a shows a schematic illustration of top view of the multiplex CARS microscopy system and the inset shows side view of the microscope. An infrared fiber laser emitting at a wavelength of 1,064 nm with an oscillation-duration of 100 ps was used as the pump laser. Another broadband super-continuum source emitting at wavelengths ranging from 460 to 2,000 nm with a temporal duration of 6 ps and a repetition rate of 20 MHz was used for Stokes laser generation. The average power of the two laser outputs was adjusted to 200 mW by the insertion of a neutral-density filter. The outputs of the pump and Stokes lasers were overlapped temporally using a dichroic beam combiner and delay line. The two lasers were focused tightly onto the samples using the 100×1.3 NA microscope objective. The CARS signals were collected using a second objective (60×0.95 NA) lens and guided into a spectroscope (SOL Instruments, SOLAR TII, MS3504i) for detection of scattered light using a CCD detector cooled to −70°C (ANDOR, Newton DU920P-BR-DD). For mapping of CARS signals, the Raman intensities were collected for each position of the laser spot focused on the target cell, which was placed on a moving piezoelectric stage. One image, consisting of an entire scan of the cell (typically an area 30 pixels wide by 30 pixels high), could be obtained in approximately 8 min, involving a dwell time. After the measurements were collected, the mapping images of different Raman bands were analyzed by comparison with

differential interference contrast images.

CARS output signal intensity ICARS is equated by a linear response with two laser powers, i.e. $I_{CARS} \propto P_{IR}\ P_{IR}\ P_{Stokes}$, where P_{IR} is excitation infrared laser power and P_{SC} is super-continuum laser power. (Fig. 2)

Budding yeasts (Saccharomyces cerevisiae W303a) were pre-cultured in 3 ml of yeast extract peptone dextrose (YPD) (Becton, Dickinson and Company) medium for 18 h at 250 rotations per minute and 30°C. The cells were then harvested and suspended in 3 ml of phosphate-buffered saline (PBS) (Gibco Life Technologies). 1 ml of the cell suspension was diluted with 2 ml of PBS and transferred to a 6-well plate (Thermo Fisher Scientific, Falcon).

Figure 1b shows a schematic illustration of the experimental setup for the plasma irradiation experiments. The NEAPP source was connected to a 60-Hz AC high-voltage power source (7 $kV_{0\text{-}p}$) with Ar gas flowing at a rate of 5 standard liters per min. The plasma plume extended about 6 mm from the exit. The slit was 20 mm wide and 0.5 mm long. The characteristics of the NEAPP source were analyzed using vacuum ultraviolet absorption spectroscopy, as previously reported.[20] The plasma density was approximately 2×10^{16} cm^{-3}, and the oxygen atom density was approximately 4×10^{14} cm^{-3}.[20] The suspension was irradiated with NEAPP at a distance of 13 mm between the bottom of the plasma source and the surface of the cell suspension for varying periods of time.

After plasma irradiation, 1 ml of the NEAPP-irradiated suspension was centrifuged, and the supernatant was replaced with fresh PBS and re-suspended. A cover glass was coated with concanavalin A (Wako), and then 2 µl of suspension was placed dropwise on the coated cover glass and then sandwiched using another cover glass. The

glass-sandwiched samples were placed on the stage of the multiplex CARS microscope for observations.

The viability of budding yeasts was assessed according to the colony forming unit method. Briefly, the suspension of NEAPP-treated budding yeast cells was diluted with PBS to an appropriate density, and then 200 μl of the diluted cell suspension was spread on a YPD agar plate and cultured at 30°C for 48 h. Cell survival was determined by counting the number of colonies formed.

Figure 3 shows the relationship between NEAPP irradiation time and cell survival. Cell survival declined in a linear manner with increasing duration of NEAPP irradiation. After 30 min of NEAPP irradiation, cell survival declined to approximately 30%.

In general, NEAPP emits UV light that generates many RONS, such as H_2O_2, NO^{2-}, and OH radicals.[21,22] The UV light can also damage the DNA of cells, leading to cell death.[23] RONS can also induce various metabolic changes in living cells that lead to cell death.[24,25] The generation of RONS could explain the cell death observed in the present study. The effect of their synergy could impact the rate of budding yeast cell death in the PBS suspension. In addition, the time threshold at which irradiation begins to induce cell death depends on the type of cells. As shown in Fig. 3, a linear relationship exists between cell survival and irradiation time, which is commonly observed.

Next, we compared the survival of budding yeast cells before and after a 30-min irradiation with NEAPP by collecting CARS spectra. Figure 4a shows CARS spectra taken before and after NEAPP irradiation. Before NEAPP treatment, several peaks exhibiting Raman shifts were clearly observed at 1440, 1602, and 1665 cm^{-1}.

After observations under bright-field illumination and a mapping measurement, these CARS signals were obtained by focusing on a point of budding yeast cells.

Vibrational peaks were observed after the non-resonant background was subtracted from the CARS spectra (Fig. 4b). CARS signals arise from the third-order nonlinear susceptibility, $\chi^{(3)}$, which is the sum of the vibrational resonant component, $\chi^{(3)}_R$, and the non-resonant electrical component, $\chi^{(3)}_{NR}$.[26] Whereas $\chi^{(3)}_{NR}$ has only a real component, $\chi^{(3)}_R$ has both real and imaginary components. It has been clearly established that spectra of the imaginary component of $\chi^{(3)}_R$, $\mathrm{Im}(\chi^{(3)}_R)$, are proportional to the spontaneous Raman spectra. Isolating the imaginary component thus provides only resonance information, which is free of the non-resonant background. These phase functions distort the measured CARS spectra; thus, the phase contributions are suppressed during spectral analysis.[27,28] In the simulated Raman spectra shown in the bottom panel of Fig. 4b, clearly identifiable bands cantered at 1440, 1602, and 1665 cm^{-1} were observed. The Raman band at 1440 cm^{-1} was assigned to CH_2 bending of the phospholipids that lipid bilayer surrounding organelles and the cell membrane other than cell walls.[16,29] The Raman band at 1665 cm^{-1} was assigned to the superposition of the C=C stretch of lipid chains and the amide I bonds of proteins.[16] As these two bands were detected simultaneously, it is reasonable to conclude that they originated from both phospholipids and proteins. The band at 1602 cm^{-1} originated from mitochondria.[16-18] The 1602 cm^{-1} Raman band is a sensitive indicator of mitochondrial metabolic activity because the Raman spectrum of ergosterol corresponds very well with the depleting spectral component in yeast that behaves together with the 1602 cm^{-1} signature when the cells are under stress.[30] Therefore, we can determine not only nutritional conditions but also the viability of budding yeast cells based on the intensity of this band, which is

aptly known as the “Raman spectroscopic signature of life”.[16-18]

Almost no intense bands were observed after 30 min of NEAPP irradiation (Fig. 4a). The 1440, 1602, and 1665 cm^{-1} bands observed in the pre-treatment spectra were almost undetectable after 30 min of irradiation. The decrease in the intensity of the Raman shift at 1602 cm^{-1} thus reflects a decrease in mitochondrial metabolic activity. The decrease in the intensity of the 1440 cm^{-1} band originating from phospholipids is possibly indicative of serious damage to the cellular membrane. A similar decrease in the intensity of the 1655 cm^{-1} band originating from the lipid bilayer was observed. As these results were due to NEAPP irradiation, we examined them from the perspective of the underlying intracellular molecular changes. Budding yeast cells were mapped using multiplex CARS microscopy to elucidate the structural and molecular effects of NEAPP. Figure 4c-e shows a differential interference contrast image (c) of untreated cells and CARS mapping of the intensity of the 1440 cm^{-1} band before (d) and after (e) NEAPP treatment for 30 min. The spectrum shown in Figure 4a was obtained from one point in Figure 4d, e. As shown in Fig. 4 (d) and (e), CARS mapping of the intensity of the 1440 cm^{-1} band originating from phospholipids reflects the shape of the cell membrane, notably, in which was observed discriminately with respect to the cell walls consisting of chitin and polysaccharide. The surrounding circular lines in the image in Fig. 4d are indicative of the cell membrane. The partly broken circular lines in the image in Fig. 4e may be indicative of disruption of the cell membrane resulting from direct plasma irradiation. A possible explanation is that oxidative species generated by plasma irradiation damaged the cell membrane. Extensive damage would be expected to lead to cell death. Although actual membrane disruption has not been proven, it has been reported that reactive oxygen species can damage proteins, the lipid bilayer, and DNA.[31]

The cell membrane was disrupted likely as a result of damage to lipids via peroxidation.

When budding yeast cells are directly irradiated with plasma, they are exposed simultaneously to charged particles, UV light emission, reactive species such as O_3 and OH radicals, as well as other excited molecular and atomic species from the plasma. The effect of short-lived radicals and long-lived chemical species such as H_2O_2 and/or UV emissions are capable of inducing sufficient intrinsic damage to the cell membrane to lead to cell death.[32,33]

Figure 5 shows a) the relationship between the intensity of the 1602 cm^{-1} band and the duration of direct NEAPP irradiation, and b) the relationship between the intensity of the 1602 cm^{-1} band and the duration of incubation of cells in PBS pre-irradiated with NEAPP for 30 min, in order to compare the direct and indirect effects of NEAPP. In the case of direct plasma irradiation, the intensity of the Raman shift at 1602 cm^{-1} decreased with increasing irradiation duration. The intensity of the 1602 cm^{-1} band was affected by the duration of irradiation rather than the duration of incubation in plasma-irradiated PBS. The short-lived radicals disappeared immediately after NEAPP irradiation.[34] The intensity of the 1602 cm^{-1} band was correlated with cell survival, as shown in Figure 3. With a 30-min NEAPP irradiation, the band intensity deceased to 30% of the initial value, and cell viability also decreased to 30% of the initial value. Thus, both phenomena were strongly correlated, indicating that the 1602 cm^{-1} band intensity is an important indicator of cell viability. Therefore, in the case of direct plasma irradiation, short-lived radicals appear to play a dominant role in the plasma-induced death of budding yeast cells.

Previous reports have suggested that the death of plasma-irradiated yeast cells is caused by the exposure to oxidative stress (e.g., H_2O_2-associated stress, leading to

apoptosis of the cells).[35,36] H_2O_2 and O_2^- radicals are relatively inert with respect to DNA.[37] OH radicals are generated from H_2O_2 by the metal-catalyzed, Fenton/Haber-Weiss reaction[37] and can damage the DNA of yeast cells.[38] Thus, the short-lived OH radicals generated by plasma can induce lethal damage in yeast. UV exposure can also damage the DNA of yeast cells.[31,39,40] The cell death was possibly caused by the UV generated from plasma. We'll undergo further investigation regarding the effects of the UV generated from plasma.

Lastly, we revealed the chemical vibrations of the cells during the NEAPP irradiation. The intensity of a band at 1602 cm^{-1} associated with mitochondrial metabolic activity of the cells were informed us the important data relevant for cell responses. Therefore, in this study, the physicochemical understanding of the biochemical effects of NEAPP irradiation on living cells using multiplex CARS microscopy is provided to the readers.

In conclusion, the survival of budding yeast cells gradually decreased as the duration of NEAPP irradiation increased. We investigated the underlying structural changes and mechanism of cell death, using label-free multiplex CARS microscopy to observe dynamically behaviors of budding yeast cells. In the present study, multiplex CARS microscopy revealed that NEAPP irradiation decreased the intensity of a band at 1602 cm^{-1} that is associated with a molecule related to mitochondrial respiration. We conclude that short-lived radicals generated by the NEAPP induced the death of these cells. Our results indicate that multiplex CARS microscopy is a useful tool for studying structural and intracellular molecular changes in living cells resulting from the application of plasmas in the medical and agricultural fields.

This study was supported in part by the MEXT KAKENHI on Innovative Areas, Japan (grant number 24108002).

References

[1] M. Laroussi, IEEE Trans. Plasma Sci., **24** (1996) 1188-1191.

[2] J. H. Noh, H. K. Baik, I. Noh, J. C. Park and I. S. Lee, Surf. Coat. Technol. **201** (2007) 5097-5101.

[3] G. Isbary, G. Morfill, H. U. Schmidt, M. Georgi, K. Ramrath, J. Heinlin, S. Karrer, M. Landthaler, T. Shimizu, B. Steffes, W. Bunk, R. Monetti, J. L. Zimmermann, R. Pompl, and W. Stolz, Br. J. Dermatol. **163** (2010) 205-207.

[4] N. Kurake, H. Tanaka, K. Ishikawa, T. Kondo, M. Sekine, K. Nakamura, H. Kajiyama, [5] F. Kikkawa, M. Mizuno, and M. Hori, Arch. Biochem. Biophys. **605** (2016) 102-108.

[6] S. Iseki, K. Nakamura, M. Hayashi, H. Tanaka, H. Kondo, H. Kajiyama, H. Kano, F. Kikkawa, and M. Hori, Appl. Phys. Lett. **100** (2012) 113702.

[7] Z. Machala, B. Tarabova, K. Hensel, E. Spetlikova, L. Sikurova, and P. Lukes, Plasma Process. Polym. **10** (2013) 649-659.

[8] S. Bekeschus, J. Kolata, C. Winterbourn, A. Kramer, R. Turner, K.D. Weltmann, B. Broker, and K. Masur, Free Radic. Res. **48** (2014) 542-549.

[9] E. A. Sosnin, E. Stoffels, M. V. Erofeev, I. E. Kieft, and S. E. Kunts, IEEE Trans. Plasma Sci. **32** (2004) 1544-1550.

[10] H. Hashizume, T. Ohta, T. Mori, S. Iseki, M. Hori, and M. Ito, Japan J. Appl. Phys. **52** (2013) 056202.

[11] F. Utsumi, H. Kajiyama, K. Nakamura, H. Tanaka, M. Mizuno, K. Ishikawa, H.

Kondo, H. Kano, M. Hori, and F. Kikkawa, Plos One. **8** (2013) e81576.

[12] M. D. Duncan, J. Reintjes, and T. J. Manuccia, Opt. Lett. **7** (1982) 350-352.

[13] J. Cheng, Y. K. Jia, G. Zheng, and X. S. Xie, Biophys. J. **83** (2002) 502-509.

[14] A. F. Palonpon, M. Sodeoka, and K. Fujita, Curr. Opt. Chem. Biol. **17** (2013) 708-715.

[15] A. F. Palonpon, J. Ando, H. Yamakoshi, K. Dodo, M. Sodeoka, S. Kawata, and K. Fujita, Nat. Prot. **8** (2013) 677-692.

[16] J. P. R. Day, K. F. Domke, G. Rago, H. Kano, H. Hamaguchi, E. M. Vartiainen, and M. Bonn, J. Phys. Chem. B. **115** (2011) 7713-7725.

[17] M. Okuno, H. Kano, P. Leproux, V. Couderc, J. P. R. Day, M. Bonn, and H. Hamaguchi, Angew. Chem. Int. Ed. **49** (2010) 6773-6777.

[18] Y. Huang, T. Karashima, M. Yamamoto, and H. Hamaguchi, Biochemistry. **44** (2005) 10009-10019.

[19] Y. Huang, T. Karashima, and H. Hamaguchi, Appl. Spectrosc. **61** (2007) 1290-1294.

[20] V. Kaliaperumal, and H. Hamaguchi, Chem. Record. **12** (2012) 567-580.

[21] M. Iwasaki, H. Inui, Y. Matsudaira, H. Kano, N. Yoshida, M. Ito, M. Hori, J. Appl. Phys. **92** (2008) 081503.

[22] S. Kalghatgi, C.M. Kelly, E. Cerchar, B. Torabi, O. Alekseev, A. Fridman, G. Friedman, and J. Azizkhan-Clifford, Plos One. **6** (2011) e16270.

[23] K. Panngom, K. Y. Baik, M. K. Nam, J. H. Han, H. Rhim, and E. H. Choi, Cell Death Dis. **4** (2013) e642.

[24] E. A. Sosnin, E. Stoffels, M. V. Erofeev, I. E. Keift, and S. E. Kunts, IEEE Trans. Plasma Sci. **32** (2004) 1544-1550.

[25] A. Costa, A. S. Dahirel, and F. Mechta-Grigoriou, Semin. Cancer Biol. **25** (2014)

23-32.

[26] S. J. Dixon, and B. R. Stockwell, Nat. Chem. Biol. **10** (2014) 9-17.

[27] C. L. Evans, E. O. Potma, and X. S. Xie, Opt. Lett. **29** (2004) 2923-2925.

[28] H. A. Rinia, M. Bonn, M. Muller, and E. M. Vartiainen, Chem. Phys. Chem. **8** (2007) 279-287.

[29] E. M. Varttiainen, J. Opt. Soc. Am. B. **9** (1992) 1209-1214.

[30] H. Segawa, M. Okuno, H. Kano, P. Leproux, V. Couderc, and H. Hamaguchi, Opt. Express. **20** (2012) 9551-9557.

[31] L. Chiu, F. H. Matsuda, T. Kobayashi, H. Torii, and H. Hamaguchi, J. Biophoto. **5** (2012) 724-728.

[32] S. G. Joshi, M. Cooper, A. Yost, M. Paff, U. K. Ercan, G. Fridman, G. Friedman, A. Fridman, and A. D. Brooks, Antimicrobiol. Agents Chemother. **55** (2011) 1053-1062.

[33] G. M. Nawkar, P. Maibam, J. H. Park, V. P. Sahi, S. Y. Lee, and C. H. Kang, Int. J. Mol. Sci. **14** (2013) 1608-1628.

[34] D. Dobrynin, G. Fridman, G. Friedman, and A. Fridman, New J. Phys. **11** (2009) 115020.

[35] R. B. Vegh, K. M. Solntsev, M. K. Kuimova, S. Cho, Y. Liang, B. L. W. Loo, L. M. Tolbert, and A. S. Bommarius, Chem. Commun. **47** (2011) 4887-4889.

[36] P. M. Ferreira and V. Costa, Redox Report. **5** (2000) 277-285.

[37] F. Madeo, E. Frohlich, M. Ligr, M. Grey, S. J. Sigrist, D. H. Wolf, and K. Frohlich, J. Cell Biol. **145** (1999) 757-767.

[38] P. M. Ferreira. V. Costa, P. Piper, and W. Mager, Mol. Microbiol. **19** (1996) 651-658.

[39] D. Frankenberg, M. F. Schwager, and R. Harbich, Int. J. Rad. Biol. **5** (1993) 511-521.

[40] W. C. Burhans, M. Weinberger, M. A. Marchetti, L. Ramachandran, G. D'Urso, and J.

A. Huberman, Mutation Res. **532** (2003) 227-243.

[41] R. D. Carratore, C. D. Croce, M. Simili, E. Taccini, M. Scavuzzo, and S. Sbrana, Mutation Res. **513** (2003) 183-191.

Figure captions

Fig. 1. Schematic illustration of (a) top view of the multiplex CARS microscopy system, (inset) side view of the microscope, and (b) the experimental setup for the plasma irradiation experiments. Abbreviations are as follows: SC, supercontinuum laser; IR, infrared laser; OF, optic fiber; M, mirror; LPF, low-pass filter; NDF, neutral-density filter; DBC, dichroic beam combiner; BPF, band-pass filter; BE, beam expander; DL, delay line; SPF, short-pass filter; CCD, charge-coupled device; OL, objective lens; SS, sample stage.

Fig. 2. Dependence of CARS signal intensity as a function of two laser output powers.

Fig. 3. Determination of the relationship between irradiation time and cell survival by counting the number of colonies formed. Data are presented as the mean ± standard error of the mean (SEM) values from four experiments.

Fig. 4. Imaging of molecular vibrational Raman signals associated with plasma-induced effects on budding yeast. (a) Spectra changes before (blue line) and after (red line) NEAPP irradiation; (b) assignment of peaks of a CARS spectrum acquired before NEAPP irradiation, Upper panel; (pale blue line) measured spectrum, (red line) fitted spectrum, (gray curved line) non-resonant background, Bottom panel; simulated Raman spectra; (c) differential interference contrast image; (d) CARS mapping of the intensity of the band at 1440 cm^{-1} before and (e) after NEAPP irradiation. Color scale of images is white for maximum intensity and dark blue for minimum intensity.

Fig. 5. Intensity of the 1602 cm^{-1} band in relation between (a) NEAPP irradiation and (b) duration time of cell-incubation in NEAPP-irradiated PBS. Data are presented as the mean ± standard error of the mean (SEM) values from four experiments.

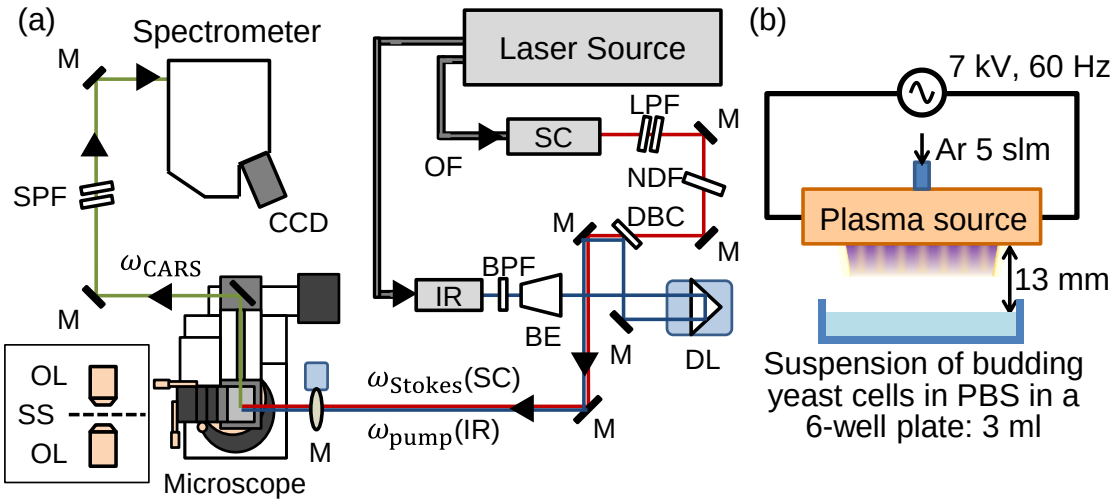

Figure 1 R. Furuta

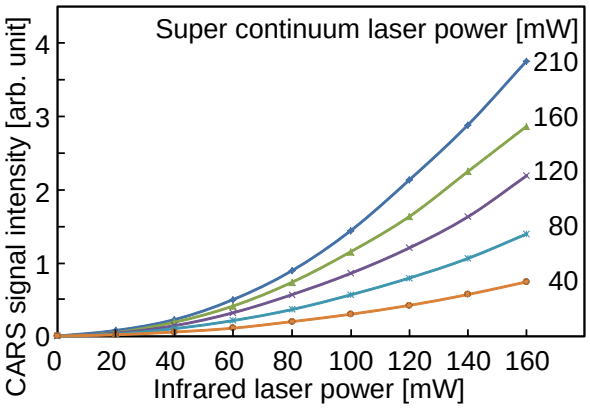

Figure 2 R. Furuta

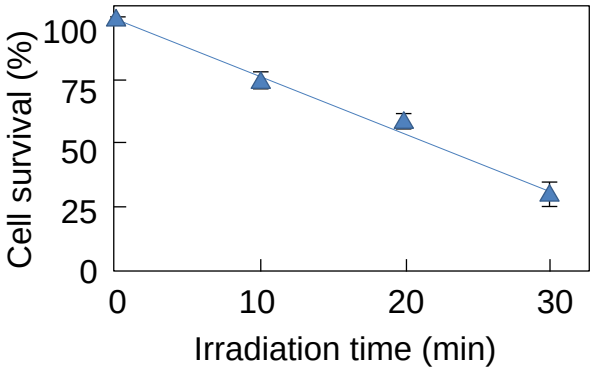

Figure 3 R. Furuta

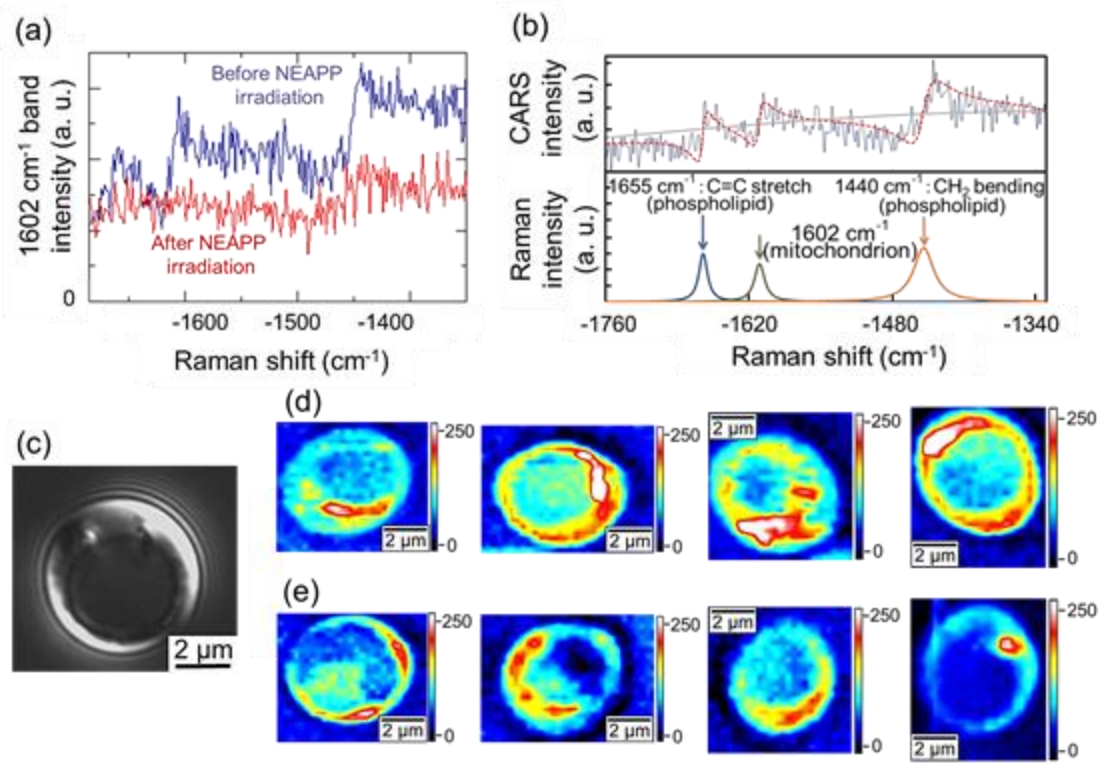

Figure 4 R. Furuta

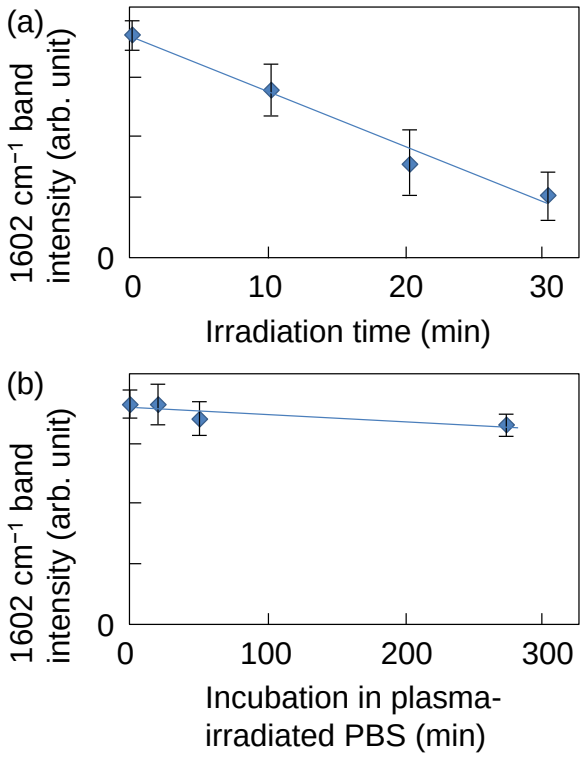

Figure 5 R. Furuta